Chinese Chemical Letters 34 (2023) 107907

Contents lists available at ScienceDirect

Chinese Chemical Letters

journal homepage: www.elsevier.com/locate/cclet

Label-free homogeneous photoelectrochemical aptasensing of $VEGF_{165}$ based on DNA-regulated peroxidase-mimetic activity of metal-organic-frameworks

Ting Hou, Ningning Xu, Xin Song, Limin Yang*, Feng Li*

College of Chemistry and Pharmaceutical Sciences, Qingdao Agricultural University, Qingdao 266109, China

ARTICLE INFO

Article history:
Received 1 August 2022
Revised 29 September 2022
Accepted 16 October 2022
Available online 18 October 2022

Keywords:
Homogenous photoelectrochemistry
Aptasensing
Label free
$VEGF_{165}$
Fe-MIL-88
Peroxidase-like activity

ABSTRACT

The application of metal-organic frameworks (MOFs) nanozymes in biosensing has been extensively investigated, however, till now there is still no report on photoelectrochemical (PEC) sensing based on enzyme memetic properties of MOFs. To further expand the utilization of MOFs nanozymes in biosensing, we developed a label-free homogenous PEC aptasensor for the detection of $VEGF_{165}$, an important cancer biomarker, based on the DNA-regulated peroxidase-mimetic activity of Fe-MIL-88, a type of MOFs. In this strategy, the peroxidase-mimetic property of MOFs is integrated with the label-free homogeneous PEC sensing approach, and highly sensitive detection of $VEGF_{165}$ is obtained with a detection limit down to 33 fg/mL, superior or comparable to the previously reported values. Moreover, this approach displays outstanding specificity, and has been successfully used to detect $VEGF_{165}$ added in diluted serum samples. As far as we know, it is the first example to employ the peroxidase-like activity of MOFs in PEC biosensing, which may find potential application in bioanalysis and early disease diagnosis.

Vascular endothelial growth factor (VEGF), a family of cell-produced signaling proteins, plays important roles in regulating angiogenesis and vascular permeabilization [1]. Among the VEGF family members, $VEGF_{165}$ is the dominating isoform and has been found to be overexpressed in human cancers such as brain tumors, breast cancer, lung cancer [2,3]. Therefore, $VEGF_{165}$, which is mainly detected in human blood samples, can be selected as a biomarker for relevant cancers. However, due to its low circulating concentrations, it is a challenge to accurately detect $VEGF_{165}$ in blood samples [4]. Thus, it is of great importance to develop precise and highly sensitive sensing methods for $VEGF_{165}$ assay.

In addition to the conventional enzyme linked immunosorbent assays (ELISA) [5], other novel analytical methods have recently been proposed for VEGF detection, including fluorescent [6,7], electrochemical [8,9], photoelectrochemical (PEC) [10–12], chemiluminescent [13], and electrochemiluminescent [14] methods. Among these strategies, PEC methods have attracted ever increasing attention, because of their distinctive merits of high sensitivity, simplicity and low cost, which result from the total dissociation of the excitation light source and the output electrochemical signal [15–17]. Moreover, PEC aptasensing combines the advantages of PEC and aptamers [18,19], and label-free PEC sensing avoids expensive labeling process [20], both exhibiting amazing momentum. In PEC assays for VEGF, DNA aptamers have also been adopted as recognition probes, which have improved affinity, specificity and stability, as well as the advantages of low cost and easiness to synthesize, as compared to the antibody-based ELISA methods [21]. However, in these PEC methods, the DNA probes were immobilized on the surface of the photoelectrodes, with the photoactive materials either intercalated into the duplexes of the DNA probes [22,23] or labeled on one strand of the DNA probes [10,11]. Such immobilization and labeling processes exhibit disadvantages of tediousness and time consuming, and more importantly it is hard to obtain bio-recognition probe modified photoelectrodes with excellent uniformity and reproducibility. Therefore, it is monumentally desirable to build both immobilization-free and label-free PEC aptasensors for VEGF detection.

Recently, inspired by the research advances in homogenous electrochemical biosensing, where both target biorecognition and signal amplification occurred in homogenous solution [24–26], our group have devoted much effort to develop homogeneous PEC sensing strategies, thus to evade the immobilization of bio-recognition probes on photoelectrode surfaces. We proposed the first truly immobilization-free PEC microRNA biosensor [27]. Along this line, we and a few other groups further simplified the procedures and proposed label-free homogeneous PEC strategies for

* Corresponding authors.
E-mail addresses: yanglimin@qau.edu.cn (L. Yang), lifeng@qau.edu.cn (F. Li).

https://doi.org/10.1016/j.cclet.2022.107907
1001-8417/

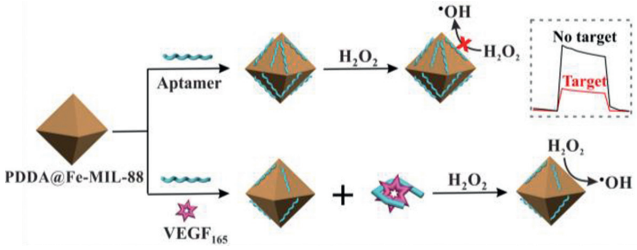

Scheme 1. Schematic illustration of the MOFs nanozyme-based label-free homogenous PEC aptasensing strategy for $VEGF_{165}$ detection.

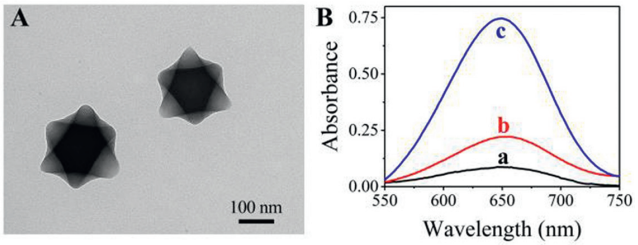

Fig. 1. (A) TEM image of the as synthesized Fe-MIL-88. (B) UV-vis absorption spectra of (a) PDDA@Fe-MIL-88 + TMB, (b) H_2O_2 + TMB, and (c) PDDA@Fe-MIL-88 + H_2O_2 + TMB, in acetate buffer (pH 4.0), in which the concentrations of Fe-MIL-88, TMB and H_2O_2 were 10 mg/mL, 6 mmol/L and 1.2 mmol/L, respectively.

the detection of different analytes [28–32], which exhibited the virtues of high sensitivity, adequate selectivity, simplicity and good repeatability. Therefore, it is worthwhile to further develop immobilization-free and label-free PEC biosensing strategies for the quantification of VEGF.

Metal-organic frameworks (MOFs), a class of nanomaterials with organic-inorganic hybrid structures, exhibit such distinguished merits as high specific surface areas, well-defined and tailorable pore sizes, abundant active sites, good stability and biocompatibility [33,34]. Besides their extended application in fields including separation, gas storage and controlled cargo release, MOFs have also demonstrated outstanding enzyme mimetic properties [35,36]. Thus, the utilization of MOFs-based nanozymes in analytical chemistry and sensing has been pursued, and MOFs nanozyme-based sensing strategies have been developed [36–40]. Despite the extensive application of MOFs nanozymes in sensing, up till now there is still no report on PEC sensing based on enzyme memetic properties of MOFs. In most MOFs-based PEC sensing approaches, MOFs were adopted as photoactive materials, precursors, hole scavenger screeners, or porous carriers of photoactive molecules [10,31,41–44]. Therefore, to take full advantage of the enzyme-memetic properties of MOFs, it is worth further exploiting MOFs nanozyme-based PEC sensing strategies.

Herein, enlightened by the above research works, we proposed a label-free homogenous PEC aptasensing strategy based on DNA-regulated enzyme-mimetic activity of Fe-MIL-88, a type of Fe-MOF with peroxidase-like activity and good dispersion in water [39,45], and attained facile and highly sensitive assay of $VEGF_{165}$. In this approach, ZnO/Ag_2S heterostructures were adopted as the photoactive materials to fabricate the photoelectrode (Fig. S1A in Supporting information). Fe-MIL-88 nanocrystals were synthesized and treated with cationic polyelectrolyte (PDDA), and the single-stranded DNA aptamers of $VEGF_{165}$ were then adsorbed on the positively charged PDDA@Fe-MIL-88 nanocrystal surface *via* electrostatic interaction. As illustrated in Scheme 1, in the absence of $VEGF_{165}$, PDDA@Fe-MIL-88 were covered with $VEGF_{165}$ aptamers to conceal the active catalytic sites, thus leading to the reduced peroxidase-memetic activity. As a result, H_2O_2 in the system remained intact, and acted as electron donors to give a relative high photocurrent under visible light irradiation (Fig. S1B in Supporting information). Whereas, if $VEGF_{165}$ was present in the system, $VEGF_{165}$ aptamers would be detached from the surface of PDDA@Fe-MIL-88 owning to the interaction with $VEGF_{165}$ to expose the active catalytic sites on Fe-MIL-88, which would catalyze the decomposition of H_2O_2 to form •OH. Thus, with the depletion of H_2O_2, the electron donors for PEC sensing, the photocurrent decreased significantly. Therefore, highly sensitive determination of $VEGF_{165}$ was realized. As far as we know, it is the first case to employ the peroxidase-like activity of MOFs in PEC biosensing.

First, the morphology of the as-synthesized Fe-MIL-88 was investigated by TEM. As can be seen, Fe-MIL-88 particles were of uniform sizes, and exhibited the unique octahedron morphology, with the average diameter of *ca.* 200 nm (Fig. 1A and Fig. S2 in Supporting information), corresponding well with those reported in literature [46,47]. The XRD pattern (Fig. S3 in Supporting information), matching well with that reported previously [47], proved that the as-synthesized Fe-MIL-88 particles had good crystalline structures.

Next, the peroxidase-like activity of the as-synthesized PDDA@Fe-MIL-88 was inspected *via* the catalyzed oxidation of 3,3′,5,5′-tetramethylbenzidine (TMB), a peroxidase substrate, in the presence of H_2O_2, to produce a blue-colored product, which has distinctive absorption at 650 nm. As shown in Fig. 1B, in the absence of either H_2O_2 or PDDA@Fe-MIL-88, relatively small absorbance was observed (curves a and b); while in the presence of PDDA@Fe-MIL-88, H_2O_2 and TMB, significantly elevated absorbance resulted (curve c), indicating the occurrence of the catalyzed oxidation of TMB, thus to verify the peroxidase-like activity of the as-synthesized PDDA@Fe-MIL-88 particles.

The morphologies of nano ZnO and ZnO/Ag_2S heterostructures were then investigated with TEM. The nano ZnO displayed laminated nanosheet structure (Fig. S4A in Supporting information), while for the ZnO/Ag_2S heterostructures, the *in-situ* fabricated Ag_2S nanoparticles, with the diameters ranging from 10 nm to 20 nm, distributed evenly on the surface of the ZnO nanosheets (Fig. S4B in Supporting information). Thus, the TEM results indicated the successful deposition of Ag_2S nanoparticles on ZnO nanosheets. Next, the number of Ag_2S layers deposited on ZnO nanosheet was optimized. It can be seen from Fig. S5 (Supporting information) that with the number of Ag_2S layers increased from 0 to 5, the photocurrent initially augmented and then declined, and the maximum photocurrent value was attained for two layers of Ag_2S. Therefore, the optimum number of Ag_2S layers was chosen to be two.

Then, EIS analysis was performed on electrodes at different modification stages to monitor the step-by-step electrode fabrication, and the EIS Nyquist plots are shown in Fig. S4C (Supporting information). It is clearly illustrated that, for bare ITO electrode, the charge transfer resistance (R_{ct}) value, related to the ability of electron transfer between $[Fe(CN)_6]^{3-/4-}$ and the electrode, and represented by the semicircle diameter of the EIS Nyquist plot (curve a), was obviously smaller than that of ITO/ZnO electrode (curve b), due to the low conductivity of ZnO, which is a metal-oxide semiconductor. Then, with Ag_2S deposited on ZnO to form ITO/ZnO/Ag_2S electrode, the R_{ct} value showed additional augmentation (curve c), because the electron transfer between the electrode and the redox probe was further impeded by the *in-situ* deposited Ag_2S nanoparticles. Therefore, the EIS results proved that the step-by-step fabrication of ITO/ZnO/Ag_2S electrodes have been accomplished.

In this work, ZnO (a semiconductor with a wide band gap) is sensitized by integrating with narrow-band-gap semiconductor Ag_2S nanoparticle to form heterostructures. To verify such sensitization effect, UV-visible absorption spectroscopy was performed on

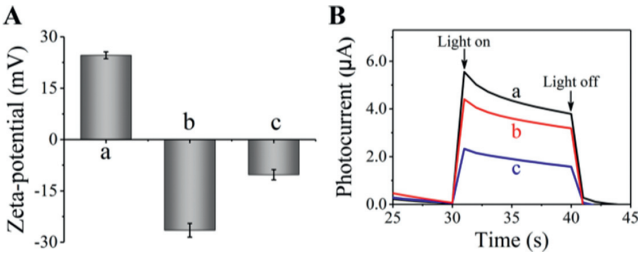

Fig. 2. (A) Zeta-potential results of (a) PDDA@Fe-MIL-88, (b) PDDA@Fe-MIL-88 + aptamer, and (c) PDDA@Fe-MIL-88 + aptamer + $VEFG_{165}$. The error bars refer to the standard deviation of five repetitive measurements. (B) Photocurrents of the reaction system under different conditions: (a) Without $VEGF_{165}$, and with (b) 0.8 pg/mL and (c) 200 pg/mL of $VEGF_{165}$.

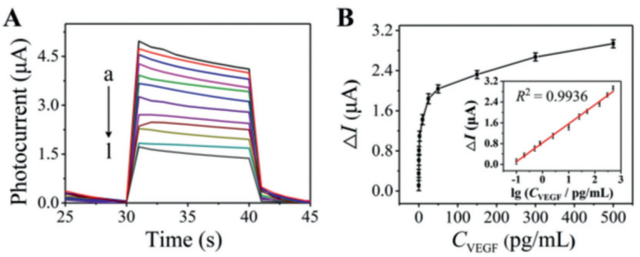

Fig. 3. (A) Photocurrent response of the biosensor to $VEGF_{165}$ with different concentrations: (a) 0, (b) 0.1, (c) 0.2, (d) 0.5, (e) 0.8, (f) 2.5, (g) 10, (h) 25, (i) 50, (j) 150, (k) 300 and (l) 500 pg/mL. (B) Plot of photocurrent change ($\Delta I = I_0 - I$) *vs.* $VEGF_{165}$ concentration, where I_0 and I are the photocurrents with and without $VEGF_{165}$, respectively. Inset: Plot of ΔI against the logarithm of $VEGF_{165}$ concentration showing a linear relationship. The error bars refer to the standard deviation of five repetitive measurements.

ITO/ZnO and ITO/ZnO/Ag_2S electrodes. As shown in Fig. S4D (Supporting information), the ITO/ZnO electrode exhibited very weak absorption in the visible light region of 400–600 nm (curve a); whereas, for ITO/ZnO/Ag_2S electrode, an obvious absorbance increase in the range of 400–600 nm was observed (curve b), demonstrating that the *in-situ* deposited Ag_2S can sensitize ZnO and move the absorption of ZnO/Ag_2S heterostructure to visible light region.

Furthermore, to investigate the optimal excitation wavelength for PEC measurements, the photocurrent response of 10 mmol/L H_2O_2 was measured using LED light sources with different wavelengths: 365, 430, 470, 530 and 627 nm. As shown in Fig. S6 (Supporting information), with the wavelength increased to 470 nm, the photocurrent showed an obvious increase and remained almost the same for the 530 and 627 nm light sources. Since longer excitation wavelength is advantageous in biosensing, 627 nm was then chosen as the optimal excitation wavelength.

To test the feasibility of the as-proposed approach for $VEGF_{165}$ detection, *zeta*-potential were measured for Fe-MIL-88 under different conditions. As illustrated in Fig. 2A, the average *zeta*-potential for PDDA@Fe-MIL-88 was 24.6 mV. In the presence of both $VEGF_{165}$ aptamer and PDDA@Fe-MIL-88, the *zeta*-potential decreased to −26.5 mV, validating the successful adsorption of $VEGF_{165}$ aptamers, which are negatively charged single-stranded DNA, on the surface of the positively charged PDDA@Fe-MIL-88. When $VEGF_{165}$ was further added into the system, the average potential changed to −10.3 mV, and this potential increase could be due to the combination of $VEGF_{165}$ and its aptamers and the subsequent displacement of $VEGF_{165}$ aptamers from the surface of PDDA@Fe-MIL-88.

Next, PEC measurements were carried out under different conditions. As demonstrated in Fig. 2B, if there was no $VEGF_{165}$ in the reaction system, a big photocurrent of *ca.* 4.4 μA was observed (curve a), because $VEGF_{165}$ aptamer adsorbed on PDDA@Fe-MIL-88 surface hindered its catalytic activity, and the electron donor (*i.e.* H_2O_2) remained intact. Whereas, in the presence of 0.8 pg/mL $VEGF_{165}$, the photocurrent decreased to 3.5 μA (curve b), suggesting that *via* the interaction between $VEGF_{165}$ and its aptamer, the aptamers were displaced from PDDA@Fe-MIL-88, whose recovered catalytic activity resulted in the consumption of H_2O_2, thus leading to a declined photocurrent. Moreover, with the concentration of $VEGF_{165}$ increased to 200 pg/mL, the photocurrent further decreased down to 1.8 μA (curve c), indicating that more $VEGF_{165}$ could displace more aptamers, leading to the increased recovery of the peroxidase-like activity of Fe-MIL-88 and increased H_2O_2 consumption, which is consistent with the mechanism proposed in Scheme 1. Therefore, the aforementioned results evidently proved the feasibility of this PEC sensing strategy for $VEGF_{165}$ detection.

To assure the best sensing performance of this PEC sensing approach, the experimental conditions were optimized. pH of the reaction system, H_2O_2 concentration, Fe-MIL-88 concentration, $VEGF_{165}$ aptamer concentration, the reaction time for the Fe-MIL-88-catalyzed H_2O_2 decomposition, the reaction time between Fe-MIL-88 and $VEGF_{165}$ aptamer, and the reaction time between $VEGF_{165}$ and its aptamer were investigated, and the optimum values were determined to be 4.0, 10.0 mmol/L, 200 μg/mL, 2.0 μmol/L, 90 min, 30 min and 60 min, respectively (Fig. S7 in Supporting information). Under these experimental conditions, the sensing performance of this $VEGF_{165}$ PEC assay was examined by adding $VEGF_{165}$ with different concentrations into the reaction system. As shown in Fig. 3A, with the $VEGF_{165}$ concentration elevated from 0 to 500 pg/mL, the corresponding photocurrent declined consequently. The photocurrent change ΔI, *i.e.*, the difference between the photocurrents in the absence and presence of $VEGF_{165}$, augmented as the $VEGF_{165}$ concentration increased from 0.1 pg/mL to 500 pg/mL (Fig. 3B), which is consistent with the sensing principle proposed in Scheme 1. Moreover, as clearly shown in the inset of Fig. 3B, a good linear relationship ($R^2 = 0.9936$) resulted between ΔI and the logarithm (to base of 10) of $VEGF_{165}$ concentration ranging from 0.1 pg/mL to 500 pg/mL, with a correlation equation of $\Delta I = 0.7316 \lg C_{VEGF} + 0.8302$, in which the units of ΔI and C_{VEGF} were μA and pg/mL, respectively. The limit of detection (LOD) was then found to be 33 fg/mL based on signal-to-noise ratio (S/N) of 3. Thus, this strategy exhibits a lower or compatible detection limit, as compared with some $VEGF_{165}$ assays reported in literature (Table S1 in Supporting information). In addition, the reproducibility of this PEC sensing strategy was evaluated, and a relative standard deviation (RSD) of 3.69% was obtained for seven parallel measurements of 2.5 pg/mL $VEGF_{165}$, demonstrating good repeatability of the PEC assay for $VEGF_{165}$ detection.

Furthermore, to study the specificity of this PEC strategy for $VEGF_{165}$ assay, PEC responses were measured by displacing $VEGF_{165}$ with four interfering proteins, namely bovine serum albumin (BSA), L-cysteine (L-Cys), thrombin (TB) and human immunoglobin G (IgG), respectively. As shown in Fig. 4, the photocur-

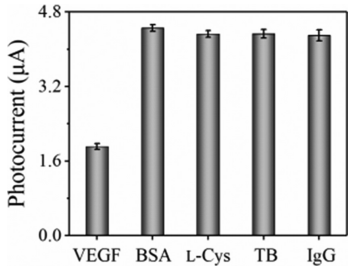

Fig. 4. Photocurrent comparison in the presence of $VEGF_{165}$ (200 pg/mL) and four interfering proteins (BSA, L-Cys, TB and IgG, all with the concentration of 5 μg/mL), respectively. The error bars refer to the standard deviation of five repetitive measurements.

Table 1
Quantification of $VEGF_{165}$ spiked in diluted human serum samples.

Sample No.	Added (pg/mL)	Detected (pg/mL) ($n = 5$)	Mean recovery[a] (%)	RSD[b] (%)
1	0.00	Not detected	–	–
2	1.00	0.97 ± 0.02	97.0	2.1
3	10.00	10.04 ± 0.37	100.4	3.7
4	50.00	50.43 ± 0.87	100.9	1.7

[a] Recovery $= (C_{detected}/C_{added}) \times 100\%$.
[b] RSD: relative standard deviation.

rent obtained in the presence of $VEGF_{165}$ (200 pg/mL) was much smaller than that acquired in the presence of BSA, L-Cys, TB or IgG, even though the concentration of the interfering proteins (5 μg/mL) is 25 times of $VEGF_{165}$ concentration. Thus, these results indicated that the PEC biosensor we proposed here has good specificity for $VEGF_{165}$ assay, and can resist the interference from coexisting interfering proteins.

Finally, the applicability of this PEC biosensor for $VEGF_{165}$ assay in real samples was studied. Before PEC measurements, the standard $VEGF_{165}$ solution was added into human serum samples diluted 100 folds by acetate buffer to give different $VEGF_{165}$ concentrations (1.00, 10.00 and 20.00 pg/mL). As shown in Table 1, the recoveries in the range of 97.0% to 104% were obtained, and the RSD was no larger than 3.92%, verifying accurate quantification of $VEGF_{165}$ in diluted serum samples.

In summary, we have developed a label-free homogenous PEC aptasensing strategy for $VEGF_{165}$ detection based on the DNA-regulated peroxidase-like activity of Fe-MIL-88, a type of MOFs. In this strategy, with enzyme-mimetic property of MOFs being integrated with the homogeneous PEC sensing approach, highly sensitive detection of $VEGF_{165}$, an important cancer biomarker, has been achieved, with a detection limit of 33 fg/mL, lower than or comparable to those previously reported. Moreover, this approach displays excellent specificity, and has been successfully adopted to quantify $VEGF_{165}$ added in diluted serum samples. Furthermore, by substituting the $VEGF_{165}$ aptamer with DNA aptamers of other targets, the detection of a variety of analytes will be facilely achieved. As far as we know, it is the first example to employ the peroxidase-like activity of MOFs in PEC biosensing, which may find potential application in bioanalysis and early disease diagnosis.

Declaration of competing interest

The authors declare that they have no known competing financial interests or personal relationships that could have appeared to influence the work reported in this paper.

Acknowledgments

This work was funded by the National Natural Science Foundation of China (Nos. 22174083 and 22076090), Shandong Provincial Natural Science Foundation (No. ZR2020ZD37), and Shandong Province Higher Educational Program for Young Innovation Talents.

Supplementary materials

Supplementary material associated with this article can be found, in the online version, at doi:10.1016/j.cclet.2022.107907.

References

[1] S. Soker, S. Takashima, H.Q. Miao, G. Neufeld, M. Klagsbrun, Cell 92 (1998) 735–745.
[2] H.F. Dvorak, J. Clin. Oncol. 20 (2002) 4368–4380.
[3] N. Gang, C. Xiaoyuan, Curr. Drug Targets 11 (2010) 1000–1017.
[4] H.W. Yang, R.Y. Tsai, J.P. Chen, et al., ACS Appl. Mater. Interfaces 8 (2016) 30845–30852.
[5] N. Rifai, M.A. Gillette, S.A. Carr, Nat. Biotechnol. 24 (2006) 971–983.
[6] S. Lu, S. Wang, J. Zhao, J. Sun, X. Yang, ACS Sens. 3 (2018) 2438–2445.
[7] Q. Chen, T. Tian, E. Xiong, P. Wang, X. Zhou, Anal. Chem. 92 (2020) 573–577.
[8] M. Amouzadeh Tabrizi, M. Shamsipur, R. Saber, S. Sarkar, Sens. Actuators B: Chem. 240 (2017) 1174–1181.
[9] X. He, X. Wang, C. Ge, et al., ACS Sens. 7 (2022) 1019–1026.
[10] Y. Fu, K. Zou, M. Liu, et al., Anal. Chem. 92 (2020) 1189–1196.
[11] H. Da, Y. Liu, M. Li, et al., Chem. Commun. 55 (2019) 8076–8078.
[12] S. Ai, H. Zeng, Y. Chai, R. Yuan, H. Liu, Sens. Actuators B: Chem. 340 (2021) 129942.
[13] W. Li, Q. Zhang, H. Zhou, et al., Anal. Chem. 87 (2015) 8336–8341.
[14] X. Long, F. Zhang, Y. He, et al., Anal. Chem. 90 (2018) 3563–3569.
[15] J. Shu, D.P. Tang, Anal. Chem. 92 (2019) 363–377.
[16] W.W. Zhao, J.J. Xu, H.Y. Chen, Chem. Soc. Rev. 44 (2015) 729–741.
[17] F.E. Osterloh, Chem. Soc. Rev. 42 (2013) 2294–2320.
[18] W.W. Zhao, J.J. Xu, H.Y. Chen, TrAC Trends Anal. Chem. 82 (2016) 307–315.
[19] Z. Li, C. Su, D. Wu, Z. Zhang, Anal. Chem. 90 (2018) 961–967.
[20] J. Xu, C. Zhao, K. Niu, Z. Gao, Y.Y. Song, Anal. Chim. Acta 1142 (2021) 1–9.
[21] J. Li, K. Sun, Z. Chen, et al., Biosens. Bioelectron. 89 (2017) 964–969.
[22] Y. Liu, H. Zeng, Y. Chai, R. Yuan, H. Liu, Chem. Commun. 55 (2019) 13729–13732.
[23] H. Da, H. Liu, Y. Zheng, R. Yuan, Y. Chai, Biosens. Bioelectron. 101 (2018) 213–218.
[24] F. Xuan, X.T. Luo, I.M. Hsing, Anal. Chem. 84 (2012) 5216–5220.
[25] F.T. Zhang, L.Y. Cai, Y.L. Zhou, X.X. Zhang, TrAC Trends Anal. Chem. 85 (2016) 17–32.
[26] L. Yang, X. Yin, B. An, F. Li, Anal. Chem. 93 (2021) 1709–1716.
[27] T. Hou, N.N. Xu, W.X. Wang, L. Ge, F. Li, Anal. Chem. 90 (2018) 9591–9597.
[28] T. Hou, N.N. Xu, W.X. Wang, L. Ge, F. Li, Biosens. Bioelectron. 141 (2019) 111395.
[29] X. Song, T. Hou, F.F. Lu, et al., Chem. Commun. 56 (2020) 1811–1814.
[30] F.F. Lu, L.M. Yang, T. Hou, F. Li, Chem. Commun. 56 (2020) 11126–11129.
[31] X.J. Liu, Y.C. Zhao, F. Li, Biosens. Bioelectron. 173 (2021) 112832.
[32] X. Wang, X. Rong, Y. Zhang, et al., Anal. Chem. 94 (2022) 3735–3742.
[33] G. Cai, P. Yan, L. Zhang, H.C. Zhou, H.L. Jiang, Chem. Rev. 121 (2021) 12278–12326.
[34] X. Jian, J. Xu, L. Yang, et al., Anal. Chem. 92 (2020) 13319–13326.
[35] X. Huang, S. Zhang, Y. Tang, et al., Coord. Chem. Rev. 449 (2021) 214216.
[36] F. Wang, L. Chen, D. Liu, et al., TrAC Trends Anal. Chem. 133 (2020) 116080.
[37] H.S. Wang, Coord. Chem. Rev. 349 (2017) 139–155.
[38] S. Li, X. Liu, H. Chai, Y. Huang, TrAC Trends Anal. Chem. 105 (2018) 391–403.
[39] X. Jian, J. Xu, Y. Wang, et al., Anal. Chem. 93 (2021) 11312–11320.
[40] H. Xu, J. Guo, L. Yang, Z. Gao, Y.Y. Song, Anal. Chem. 93 (2021) 9486–9494.
[41] G.Y. Zhang, Y.H. Zhuang, D. Shan, et al., Anal. Chem. 88 (2016) 11207–11212.
[42] W.W. Zhan, Q. Kuang, J.Z. Zhou, et al., J. Am. Chem. Soc. 135 (2013) 1926–1933.
[43] G. Zhang, D. Shan, H. Dong, et al., Anal. Chem. 90 (2018) 12284–12291.
[44] S. Zhou, J. Guo, Z. Dai, et al., Anal. Chem. 93 (2021) 12067–12074.
[45] Y.L. Liu, X.J. Zhao, X.X. Yang, Y.F. Li, Analyst 138 (2013) 4526–4531.
[46] K.M.L. Taylor-Pashow, J. Della Rocca, Z. Xie, S. Tran, W. Lin, J. Am. Chem. Soc. 131 (2009) 14261–14263.
[47] Y.L. Liu, W.L. Fu, C.M. Li, C.Z. Huang, Y.F. Li, Anal. Chim. Acta 861 (2015) 55–61.